

Toward wafer-scale diamond nano- and quantum technologies ^{EP}

Cite as: APL Mater. 7, 011108 (2019); <https://doi.org/10.1063/1.5067267>

Submitted: 16 October 2018 • Accepted: 02 January 2019 • Published Online: 28 January 2019

 Richard Nelz, Johannes Görlitz, Dennis Herrmann, et al.

COLLECTIONS

 This paper was selected as an Editor's Pick



View Online



Export Citation



CrossMark

ARTICLES YOU MAY BE INTERESTED IN

[Quantum computer based on color centers in diamond](#)

Applied Physics Reviews **8**, 011308 (2021); <https://doi.org/10.1063/5.0007444>

[Spin measurements of NV centers coupled to a photonic crystal cavity](#)

APL Photonics **4**, 120803 (2019); <https://doi.org/10.1063/1.5120120>

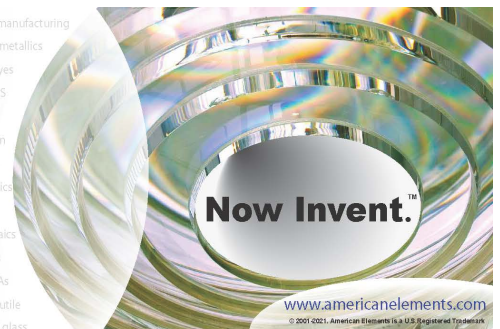
[Introduction to quantum optimal control for quantum sensing with nitrogen-vacancy centers in diamond](#)

AVS Quantum Science **2**, 024701 (2020); <https://doi.org/10.1116/5.0006785>



yttrium iron garnet glassy carbon beamsplitters fused quartz additive manufacturing
 zeolites III-IV semiconductors gallium lump copper nanoparticles organometallics
 nano ribbons barium fluoride europium phosphors photonics infrared dyes
 epitaxial crystal growth ultra high purity materials transparent ceramics CIGS
 cerium oxide polishing powder surface functionalized nanoparticles MRE grade materials thin film
 silver nanoparticles perovskites MOCVD beta-barium borate rare earth metals quantum dots
 osmium scintillation Ce:YAG refractory metals laser crystals
 anode lithium niobate InAs wafers dysprosium pellets MOFs AuNPs chalcogenides ZnS CdTe perovskite crystals transparent ceramics

The Next Generation of Material Science Catalogs



Toward wafer-scale diamond nano- and quantum technologies

Cite as: APL Mater. 7, 011108 (2019); doi: 10.1063/1.5067267

Submitted: 16 October 2018 • Accepted: 2 January 2019 •

Published Online: 28 January 2019



View Online



Export Citation



CrossMark

Richard Nelz,¹  Johannes Görlitz,¹ Dennis Herrmann,¹ Abdallah Slablab,¹ Michel Challier,¹ Mariusz Radtke,¹ Martin Fischer,² Stefan Gsell,² Matthias Schreck,³  Christoph Becher,¹  and Elke Neu^{1,a)} 

AFFILIATIONS

¹Universität des Saarlandes, Fakultät NT, Physik, 66123 Saarbrücken, Germany

²Augsburg Diamond Technology GmbH, 86159 Augsburg, Germany

³Universität Augsburg, Institut für Physik, 86135 Augsburg, Germany

^{a)}Electronic mail: elkenu@physik.uni-saarland.de

ABSTRACT

We investigate native nitrogen vacancy (NV) and silicon vacancy (SiV) color centers in a commercially available, heteroepitaxial, wafer-sized, mm thick, single-crystal diamond. We observe single, native NV centers with a density of roughly 1 NV per μm^3 and moderate coherence time ($T_2 = 5 \mu\text{s}$) embedded in an ensemble of SiV centers. Using low temperature luminescence of SiV centers as a probe, we prove the high crystalline quality of the diamond especially close to the growth surface, consistent with a reduced dislocation density. Using ion implantation and plasma etching, we verify the possibility to fabricate nanostructures with shallow color centers rendering our material promising for fabrication of nanoscale sensing devices. As this diamond is available in wafer-sizes up to 100 mm, it offers the opportunity to up-scale diamond-based device fabrication.

© 2019 Author(s). All article content, except where otherwise noted, is licensed under a Creative Commons Attribution (CC BY) license (<http://creativecommons.org/licenses/by/4.0/>). <https://doi.org/10.1063/1.5067267>

Diamond nanostructures are of significant importance for various applications in science and industry including nanomechanical devices,¹ photonics² and sensing.³ A major challenge for most of these applications is the scalability of the fabrication process predominantly due to a lack of large area single-crystal diamonds (SCDs) with good crystalline quality and high purity. Manufacturing synthetic SCD on a wafer scale has been an active field of research^{4,5} leading to the commercial availability of SCD with a diameter of ≈ 100 mm recently. This progress opens the road toward up-scaling the fabrication of SCD nanostructures especially for diamond related sensing applications.⁶ Color centers in SCD, in particular, the negatively charged nitrogen vacancy (NV) center in nanostructures, have been extensively used to sensitively measure, e.g., magnetic fields in the last decade. Single color centers allow for sensing with high spatial resolution and offer bright, photostable photoluminescence (PL). In addition, NV centers provide highly coherent, controllable spin states³ and show optically detected magnetic resonance

(ODMR) enabling to read out their spin states via PL detection. As a consequence, even single NV centers can serve as quantum-enhanced sensors. Magnetic field imaging using NV centers has various applications ranging from material characterization in superconductors⁷ or magnetic materials for spintronics⁸ to life science applications where nuclear magnetic resonance detection of single proteins is of interest.⁹ Recently, silicon vacancy (SiV) centers emerged as alternative enabling all optical sensing of temperatures using their narrow electronic transitions.¹⁰

We here demonstrate the basic applicability of commercial, wafer-sized SCD for quantum technology applications. To this end, we demonstrate coherent manipulation of single native NV center spins in the SCD, while we use low-temperature spectroscopy of SiV center PL as a probe to prove the high crystalline quality of the material. In addition, we implant shallow NV centers (depth ≈ 10 nm), indispensable for nanoscale sensing, and investigate their suitability for quantum sensing applications.

Furthermore, we apply reactive ion etching to the material to illustrate routes toward up-scaling of diamond-related nanofabrication.

We use (100) oriented SCD from AuDiaTec (Augsburg Diamond Technology GmbH) synthesized in a microwave plasma enhanced chemical vapor deposition process based on a methane/hydrogen (CH_4/H_2) gas mixture at a temperature $>1000^\circ\text{C}$. H_2 was purified by passing it through a AgPd membrane, while the used CH_4 had a purity of 99.9995%. As a consequence, we estimate the nitrogen (N_2) concentration in the gas phase to be <0.5 ppm. The Ir/YSZ (yttria stabilized zirconia)/Si substrate was removed by chemical etching and grinding before the diamond wafer was cut into pieces of $3\text{ mm} \times 3\text{ mm}$ using a pulsed IR laser. The SCDs are 1.3 mm thick. For our experiments, we use the crystals with the as grown surface. SCD synthesis at AuDiaTec is based on the technology developed at the University of Augsburg. As described in Ref. 5, successful scaling of heteroepitaxial nucleation and growth to 100 mm wafer-size was achieved by the use of the multilayer substrate Ir/YSZ/Si. During heteroepitaxial growth of thick (mm) SCD, the dislocation density decreases proportional to the inverse of the SCD layer thickness indicating high crystalline quality for this material at the growth surface.⁵ Previous studies⁵ furthermore reveal a high homogeneity of the crystalline quality using Raman scattering and X-ray diffraction.

To investigate PL and perform spin manipulation of NV centers, we use a home-built confocal microscope (numerical aperture NA 0.8, 532 nm laser excitation) where confocal filtering of the PL is ensured by using a single mode optical fiber. To quantify the PL intensity, we use highly efficient photon counters (Excelitas SPCM-AQRH-14, quantum efficiency $\approx 70\%$). In addition, we use a grating spectrometer (Acton Spectra Pro 2500, Pixis 256OE CCD) to record the PL spectrum. To measure PL lifetimes, we employ time correlated photon counting (PicoQuant, PicoHarp 300) and pulsed laser excitation (NKT EXW-12, pulse length $\approx 50\text{ ps}$, wavelength $527\text{--}537\text{ nm}$). The setup is equipped with a microwave source and an amplifier (Stanford Research Systems, SG384 and Mini Circuits, ZHL-42W+) for spin-manipulation of NV centers. To investigate SiV centers, we use a second confocal microscope (numerical aperture NA 0.9) embedded into a liquid helium flow cryostat employing a titanium-sapphire laser (Matisse, TX) at 690 nm as an excitation source. For confocal filtering, a single mode optical fiber is used. PL spectra of SiV centers are recorded using a grating spectrometer (Jobin Yvon, Horiba, Grating: 1800 g/mm).

We now discuss the PL results from our SCD under continuous laser excitation at 532 nm . Close ($<5\text{ }\mu\text{m}$) to the nucleation side, we observe very bright PL consisting of a broad background as well as distinctive NV and SiV PL. By contrast, PL maps recorded in a wavelength range from 680 nm to 720 nm from planes parallel and closer to the growth surface show bright, distinguishable spots [see Fig. 1(a)]. The spots clearly show PL spectra of NV centers [see Fig. 1(b)], constituting the first observation of individual native NV centers in heteroepitaxial SCD. Additionally, these PL spectra reveal the presence of homogeneously distributed SiV centers which,

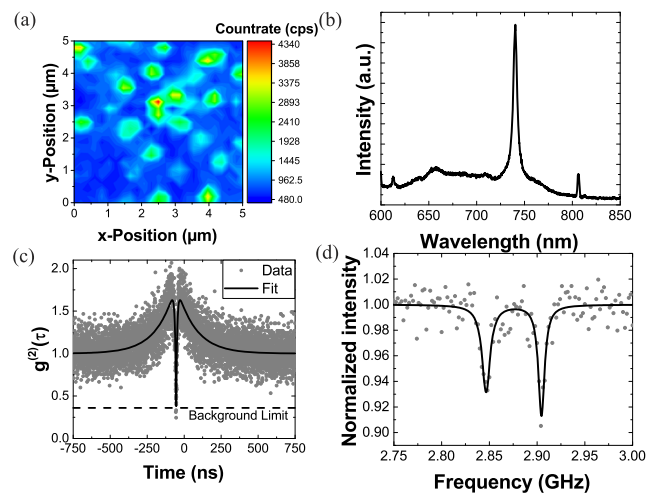


FIG. 1. (a) PL map of the SCD (detected wavelength range 680 nm – 720 nm) showing ≈ 25 bright spots which all have NV PL. (b) Room temperature PL spectrum of one of these NVs. Bright SiV zero phonon line (ZPL) is visible leading to the background measured in the PL map in (a) despite spectral filtering. The narrow PL line observed at 805 nm is most probably connected to the SiV ensemble,^{14,15} while the peak at 610 nm corresponds to the second order Raman scattering of diamond. (c) $g^{(2)}$ -measurement of one of the NVs. A clear anti-bunching is visible. $g^{(2)}(0)$ is only limited by the background of the SiV ensemble (see the [supplementary material](#)). (d) ODMR measurement of single NV showing a background-corrected contrast C above 10% (external magnetic field approximately 11 G).

despite spectral filtering, influence observation of single NV centers as background.

To test the applicability of the material for NV-based quantum technologies, we investigate single, native NV centers in the highest-quality region, namely, the first micrometers below the growth surface. To prove the observation of single NV centers, we measure second order photon correlations $g^{(2)}$ [see Fig. 1(c)]. We achieve a signal-to-background ratio of less than 4, limited by SiV PL. Nevertheless, these measurements clearly show single photon emission of NV centers, while the SiV ensemble PL limits $g^{(2)}(0)$ (see the [supplementary material](#)). From PL maps recorded at different positions of the sample [see Fig. 1(a)], we determine a homogenous NV density of $\approx 1\text{ NV per }\mu\text{m}^3$ equivalent to a concentration of $\approx 0.005\text{ ppb}$. This value is in reasonable accordance with the density estimated from the nitrogen impurity concentration in the feed gases (for details, see the [supplementary material](#)). Subsequently, we perform photoluminescence lifetime imaging of individual NV centers (for data, see the [supplementary material](#)). The NV centers show on average a lifetime of $12.3(6)\text{ ns}$ which agrees well with the lifetime in bulk SCD.¹¹ This finding rules out quenching, e.g., due to structural defects associated with the incorporation of silicon impurities¹² as well as quenching via potential near-field energy transfer between NV and SiV centers.¹³ Furthermore, we perform ground state ODMR measurements of single NVs. We obtain the ODMR-spectrum in Fig. 1(d) with narrow resonances (an external magnetic field of 11 G applied) and a contrast exceeding 10%. The zero-field-splitting of 2.876 GHz indicates low strain close

to the growth surface which would otherwise shift or split the resonance. Spin-Echo measurements of single NV centers at randomly chosen positions in the sample consistently show a coherence time of $T_2 = 5(1) \mu\text{s}$, proving homogenous properties of the NV centers in the SCD.

To further characterize the crystalline quality of the SCD, we study the SiV ensemble in detail. Hereby, we focus on the fine structure of the SiV zero phonon line (ZPL) which is a meaningful measure of the crystalline quality as strain shifts and broadens the fine structure components in the ensemble. Consequently, we measure the ZPL fine structure at 10 K in different depths along the growth direction (see Fig. 2). We observe a clear fine structure close to the growth surface, while ZPL broadening completely masks the fine structure deeper in the SCD toward the nucleation side where the growth started. We expect the ZPL to broaden linearly with dislocation density.¹⁶ To verify this fact, we fit the linewidth using a $1/\text{layer thickness}^n$ dependence. We obtain $n \approx 1$ which is in good agreement with the predicted dislocation density evolution during growth which should lead to an estimated density of dislocations of $\approx 10^7 \text{ cm}^{-2}$ close to the growth surface.⁵ In this area, we observe a fitted linewidth of 61.2(5) GHz (for details, see the [supplementary material](#)). Our observed linewidths are thus only roughly a factor of 6 higher than in high-quality, thin, homoepitaxial SCD films¹⁷ witnessing high crystalline quality.

Efficient nanoscale sensing using color centers in SCD typically requires shallow NV centers (<50 nm below the surface) incorporated into dedicated nanostructures, e.g., nanopillars.⁶ To test the usability of our novel SCD material, we shallowly implant nitrogen ions with an implantation energy of 6 keV and doses of 1.5 and $3 \times 10^{11} \text{ cm}^{-2}$ to form a NV layer 10 nm below the SCD surface. After annealing the sample, PL maps reveal homogenous creation of the NV layer across the sample for both doses. PL spectra from the implanted layer [see Fig. 3(a)] show strong NV PL, while weaker PL below 640 nm corresponds to phononic side bands originating from neutral NV centers; strong SiV PL is still visible. Due to the enhanced number of NVs, their PL is more pronounced, whereas the SiV PL remains mainly unchanged.

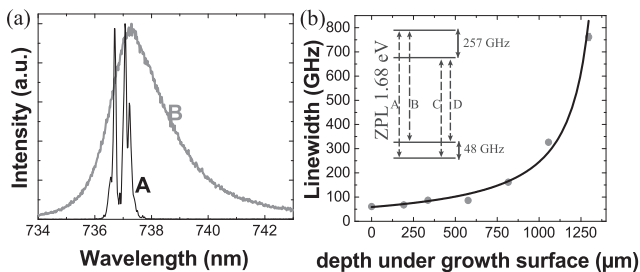


FIG. 2. Probing strain in the SCD material via SiV PL: (a) PL spectra of the SiV ensemble at 10 K. Close to the growth surface, a clear fine structure is visible (black curve A), while the ZPL continuously broadens along the growth direction. Closer to the substrate, broadening completely masks the fine structure components (gray curve B). (b) Linewidth of the transition C along the growth direction of the diamond. Inset: SiV level scheme according to Ref. 18.

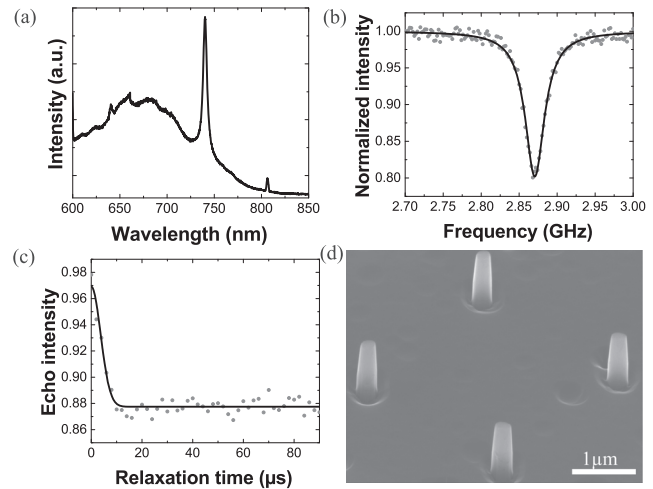


FIG. 3. (a) PL spectrum of the implanted NV ensemble. A clear NV^- as well as minor NV^0 spectrum is visible, while SiV PL remains unchanged. (b) ODMR spectrum without external magnetic field strongly broadened due to strong microwave pumping of the transition (unbroadened linewidth 10.67 MHz, $C = 20\%$). (c) Spin-echo-measurement of the implanted NV centers, fitted employing the formalism derived in Ref. 22. The coherence time is $T_2 = 5.2(3) \mu\text{s}$. (d) Scanning electron microscopy image of nanopillars etched into the growth surface of the SCD. The cylindrical pillars have a diameter of $\approx 200 \text{ nm}$ and a height of $\approx 1 \mu\text{m}$.

The PL lifetime of the implanted NV centers is longer than the native NV centers' lifetime due to their proximity to the surface. We find $\tau = 17 \text{ ns}$, typical for shallowly implanted NV centers.⁶ To demonstrate the usability of the NV center ensemble for magnetic sensing, we measure ODMR without applying an external magnetic field which shows a contrast of $C = 20\%$ [see Fig. 3(b)] at 2.871(2) GHz. Power broadening for the ODMR resonance occurs because of the strong microwave field necessary to saturate the ground state spin transition in the ensemble. To estimate the unbroadened linewidth, we follow Ref. 19 and obtain a linewidth of 10.67 MHz (see the [supplementary material](#)). Rabi oscillations of a sub-ensemble of the implanted NV centers using a bias magnetic field of 38 G confirm coherent manipulation of the spins. The spin coherence time $T_2 = 5.2(3) \mu\text{s}$ of the implanted NV centers is comparable to T_2 for the native NVs [see Fig. 3(c)] and consistent for positions several mm apart. Consequently, we assume that T_2 is limited by the properties of our SCD. Often, the concentration of substitutional nitrogen $[\text{N}]^s$ limits T_2 .³ However, as the estimated concentration of $[\text{N}]^s$ is in the ppb range for our SCD, we would expect T_2 to be at least an order of magnitude higher than observed. We also exclude minor concentrations of compensated boron acceptors as the source of decoherence. A possible spin bath reducing T_2 for the observed native NV centers might arise from various paramagnetic, silicon-containing defects in the material including neutral SiV centers and optically inactive silicon-hydrogen complexes.²⁰ Furthermore, vacancy complexes especially divacancies have been identified as a source of decoherence for implanted NV centers recently.²¹ We tentatively suggest that

vacancy complexes forming at dislocations might reduce T_2 in our material.

Another important test for the material is to manufacture well-defined and stable nanostructures by reactive ion etching like, e.g., nanopillars or scanning probes.⁶ Such photonic nanostructures significantly enhance photon rates from single color centers, consequently boosting sensor sensitivity.²³ We use the pristine growth surface (2.2 nm rms roughness, area $2\ \mu\text{m} \times 2\ \mu\text{m}$) to etch nanopillars in an inductively coupled reactive ion etching plasma (Ar/O₂, 50 sccm each, 18.9 mTorr, 500 W ICP, 200 W RF power) enabling highly anisotropic etching of SCD. The nanopillars have an almost cylindrical shape with a diameter of $\approx 200\ \text{nm}$ and a height of $\approx 1\ \mu\text{m}$ [see Fig. 3(d)] closely resembling scanning probes optimized for high sensitivity magnetometry.²³ The surface roughness remains mainly unchanged ($<4\ \text{nm}$ rms roughness, area $2\ \mu\text{m} \times 2\ \mu\text{m}$) with no etchpits forming. We note that considering the estimated density of dislocations, the probability to find a dislocation within an individual pillar is only $\approx 1\%$ indicating the suitability of our high quality heteroepitaxial SCD for the production of quantum technology devices. Thus, our wafer-sized SCD opens up the way for up-scaling nanofabrication of NV center-related structures for various applications.

In conclusion, we show that our wafer-sized, heteroepitaxial SCD contains single, native NV centers with a homogeneous density of roughly 1 NV per μm^3 embedded in an ensemble of SiV centers. Native NVs show moderate coherence time of $T_2 = 5\ \mu\text{s}$ and are suitable for ODMR-related sensing applications. A clear fine structure of the SiV ZPL close to the growth surface witnesses low strain and high crystalline quality. Additionally, we shallowly implant NV centers as required for nanoscale sensing and demonstrate the fabrication of nanopillars into the pristine SCD growth surface.

The outstanding advantage of the present material system is its commercial availability and superior size, potentially enabling up-scaling of nanostructure fabrication for sensing and consequently reducing manufacturing cost for SCD-based devices. Due to wafer-scale growth, also the cost per carat can be reduced by potentially one order of magnitude compared to present high-purity SCD. Consequently, the material has the potential to eliminate a bottle neck in SCD-based technologies. Challenges arise from moderate NV coherence times in the material and the detrimental influence of the SiV PL on NV spin readout limiting the usability of NV centers for sensing. To reduce the incorporation of silicon, we envisage overgrowing millimeter-thick SCD wafers after removal of the Ir/YSZ/Si substrate since the Si-wafer is the main source of silicon in the process. For many applications, only thin active layers ($<10\ \mu\text{m}$) are required. As a consequence, a slow growth rate and process conditions for optimized crystal quality can be chosen. We anticipate that this approach will considerably improve NV coherence in the active zone. Nevertheless, the observed native NV centers are already useful for sensing using ODMR resonances shifts to detect magnetic fields with moderate strength, e.g., when performing failure analysis of electric circuits²⁴ or imaging of domain walls in thin ferromagnetic films applicable in

spintronics.⁸ Similarly, implanted ensembles of NV centers are suitable for wide-field imaging of magnetic particles in living cells.²⁵

See [supplementary material](#) for details about nitrogen incorporation, background determination of the $g^{(2)}$ -measurements, fitting of the SiV PL, PL lifetime maps, and estimation of the power broadening.

This research has been funded via the NanoMatFutur program of the German Ministry of Education and Research (BMBF) under Grant No. FKZ13N13547. We acknowledge funding via a PostDoc fellowship of the Daimler and Benz Foundation. We thank Jörg Schmauch for recording SEM images as well as Dr. Rene Hensel for the use of the ICP-RIE and assistance.

REFERENCES

- 1 J. Teissier, A. Barfuss, P. Appel, E. Neu, and P. Maletinsky, *Phys. Rev. Lett.* **113**, 020503 (2014).
- 2 I. Aharonovich and E. Neu, *Adv. Opt. Mater.* **2**, 911 (2014).
- 3 L. Rondin, J.-P. Tetienne, T. Hingant, J.-F. Roch, P. Maletinsky, and V. Jacques, *Rep. Prog. Phys.* **77**, 056503 (2014).
- 4 H. Yamada, A. Chayahara, Y. Mokuno, Y. Kato, and S. Shikata, *Appl. Phys. Lett.* **104**, 102110 (2014).
- 5 M. Schreck, S. Gsell, R. Brescia, and M. Fischer, *Sci. Rep.* **7**, 44462 (2017).
- 6 P. Appel, E. Neu, M. Ganzhorn, A. Barfuss, M. Batzer, M. Gratz, A. Tschöpe, and P. Maletinsky, *Rev. Sci. Instrum.* **87**, 063703 (2016).
- 7 L. Thiel, D. Rohner, M. Ganzhorn, P. Appel, E. Neu, B. Müller, R. Kleiner, D. Koelle, and P. Maletinsky, *Nat. Nano* **11**, 677 (2016).
- 8 J.-P. Tetienne, T. Hingant, J.-V. Kim, L. H. Diez, J.-P. Adam, K. Garcia, J.-F. Roch, S. Rohart, A. Thiaville, D. Ravelosona, and V. Jacques, *Science* **344**, 1366 (2014).
- 9 I. Lovchinsky, A. O. Sushkov, E. Urbach, N. P. de Leon, S. Choi, K. De Greve, R. Evans, R. Gertner, E. Bersin, C. Müller, L. McGuinness, F. Jelezko, R. L. Walsworth, H. Park, and M. D. Lukin, *Science* **351**, 836 (2016).
- 10 C. T. Nguyen, R. E. Evans, A. Sipahigil, M. K. Bhaskar, D. D. Sukachev, V. N. Agafonov, V. A. Davydov, L. F. Kulikova, F. Jelezko, and M. D. Lukin, *Appl. Phys. Lett.* **112**, 203102 (2018).
- 11 N. B. Manson, J. P. Harrison, and M. J. Sellars, *Phys. Rev. B* **74**, 104303 (2006).
- 12 A. Bolshakov, V. Ralchenko, V. Sedov, A. Khomich, I. Vlasov, A. Khomich, N. Trofimov, V. Krivobok, S. Nikolaev, R. Khmelnski, and V. Saraykin, *Phys. Status Solidi A* **212**, 2525 (2015).
- 13 D. Gatto Monticone, F. Quercioli, R. Mercatelli, S. Soria, S. Borini, T. Poli, M. Vannoni, E. Vittone, and P. Olivero, *Phys. Rev. B* **88**, 155201 (2013).
- 14 E. Neu, M. Fischer, S. Gsell, M. Schreck, and C. Becher, *Phys. Rev. B* **84**, 205211 (2011).
- 15 S. Lindner, A. Bommer, A. Muzha, A. Krueger, L. Gines, S. Mandal, O. Williams, E. Londero, A. Gali, and C. Becher, *New J. Phys.* **20**, 115002 (2018).
- 16 V. Hizhnyakov and P. Reineker, *J. Chem. Phys.* **111**, 8131 (1999).
- 17 E. Neu, C. Hepp, M. Hauschild, S. Gsell, M. Fischer, H. Sternschulte, D. Steinmüller-Nethl, M. Schreck, and C. Becher, *New J. Phys.* **15**, 043005 (2013).
- 18 C. Arend, J. N. Becker, H. Sternschulte, D. Steinmüller-Nethl, and C. Becher, *Phys. Rev. B* **94**, 045203 (2016).
- 19 A. Dréau, M. Lesik, L. Rondin, P. Spinicelli, O. Arcizet, J.-F. Roch, and V. Jacques, *Phys. Rev. B* **84**, 195204 (2011).
- 20 U. F. S. D'Haenens-Johansson, A. M. Edmonds, M. E. Newton, J. P. Goss, P. R. Briddon, J. M. Baker, P. M. Martineau, R. U. A. Khan, D. J. Twitchen, and S. D. Williams, *Phys. Rev. B* **82**, 155205 (2010).

²¹F. F. de Oliveira, D. Antonov, Y. Wang, P. Neumann, S. A. Momenzadeh, T. Häußermann, A. Pasquarelli, A. Denisenko, and J. Wrachtrup, *Nat. Commun.* **8**, 15409 (2017).

²²L. Childress, M. V. Gurudev Dutt, J. M. Taylor, A. S. Zibrov, F. Jelezko, J. Wrachtrup, P. R. Hemmer, and M. D. Lukin, *Science* **314**, 281 (2006).

²³P. Fuchs, M. Challier, and E. Neu, *New J. Phys.* **20**, 125001 (2018).

²⁴A. Nowodzinski, M. Chipaux, L. Toraille, V. Jacques, J.-F. Roch, and T. Debuisschert, *Microelectron. Reliab.* **55**, 1549 (2015).

²⁵D. Le Sage, K. Arai, D. R. Glenn, S. J. DeVience, L. M. Pham, L. Rahn-Lee, M. D. Lukin, A. Yacoby, A. Komeili, and R. L. Walsworth, *Nature* **496**, 486 (2013).